Journal of Geochemical Exploration 184 (2018) 150–157

Contents lists available at ScienceDirect

Journal of Geochemical Exploration

journal homepage: www.elsevier.com/locate/gexplo

Selection of an elemental association related to mineralization using spatial analysis

Renguang Zuo

State Key Laboratory of Geological Processes and Mineral Resources, China University of Geosciences, Wuhan 430074, China

ARTICLE INFO

Keywords:
Geochemical prospecting
Elemental association
Spatial analysis
Multifractal spectrum
Receiver operating characteristic

ABSTRACT

Geochemical exploration plays a significant role in mineral exploration because it can help lead to the discovery of various types of mineral deposits. For a given geochemical exploration dataset, a number of elements are typically measured synchronously. Of these elements, several are associated with mineralization that can guide exploration, and the remaining elements may reflect other geological processes or events. How to identify elemental associations that are spatially correlated with locations of mineralization using spatial statistics, was addressed in this study. To do so, a hybrid method that combines the multifractal spectrum and the receiver operating characteristic (ROC) curve was applied. The spatial distribution characteristics of geochemical patterns were first investigated through multifractal analysis, in which enriched elements can be identified with a symmetry index R of > 1. These enriched elements were further examined using ROC to evaluate the spatial correlations between geochemical patterns and locations of mineral deposits. The elements with areas under curve (AUC) and Z_{AUC} values obtained from the ROC curve > 0.5 and 1.96, respectively, which represent strong positive spatial relationships with mineralization, comprise the identified elemental association for locating mineralization. This hybrid method provides objective selection criteria for elemental associations related to mineralization based on spatial statistics. A case study was conducted in southwestern Fujian Province, China to demonstrate the capability of the proposed method. An integrated geochemical map based on the identified elemental association related to skarn-type Fe mineralization was produced and can be employed as a reference in further mineral exploration in the study area. However, the geological environment for the formation of mineralization should be considered in conjunction with the proposed approach.

1. Introduction

Several geochemical mapping datasets are available through the Association of Applied Geochemists (AAG) website (www.appliedgeochemists.org). For an individual geochemical dataset, several elements are typically measured together. For instance, the Forum of European Geological Surveys (FOREGS) dataset, launched in 1996, includes 54 parameters (Darnley et al., 1995); the Chinese National Geochemical Mapping Project, initiated in 1978, includes 39 major and trace elements (Xie et al., 1997); and the National Geochemical Survey of Australia (NGSA) project dataset comprises measurements for 60 elements (de Caritat et al., 2010). Many elements are spatially associated with specific types of mineralization that can guide geoscientists to discover mineral deposits, whereas the remaining elements may reflect other geological processes or events unrelated to mineralization. Identification of elemental associations that are spatially correlated with locations of mineralization based on spatial analysis was addressed in this study.

There are three approaches to identify elemental associations for a specific type of mineral deposit. The first is a traditional approach based on studying the geological characteristics of known mineral deposits to identify the main ore-forming elements and associated elements. For example, by studying typical mineral deposits, Cheng (2007) identified Sn–As–Cu–Pb–Zn–Cd as the elemental association related to Tin mineral deposits in Gejiu district, Yunan Province, China. Such elemental association can represent the variety of mineralization in this area because some elements represent ore minerals and others are gauge minerals; Zuo et al. (2009) recognized Cu–Mo–Pb–Zn as an elemental association related to porphyry Cu–Mo mineralization in the Gangdese belt of Tibet, China. The second approach is based on multivariate analysis of geochemical exploration data to extract meaningful elemental factors reflecting mineralization (e.g., Grunsky, 1986; Harris et al., 1999, 2000; Grunsky et al., 2013, 2014, 2017; Mueller and Grunsky, 2016; Chen et al., 2016; Zuo et al., 2009, 2013; Parsa et al., 2017c; Zuo et al., 2013; Zuo, 2017). For instance, Grunsky and Smee (1999) applied principal component analysis (PCA) to extract distinct

E-mail address: zrguang@cug.edu.cn.

http://dx.doi.org/10.1016/j.gexplo.2017.10.020
Received 25 March 2017; Received in revised form 5 October 2017; Accepted 26 October 2017
Available online 27 October 2017
0375-6742/

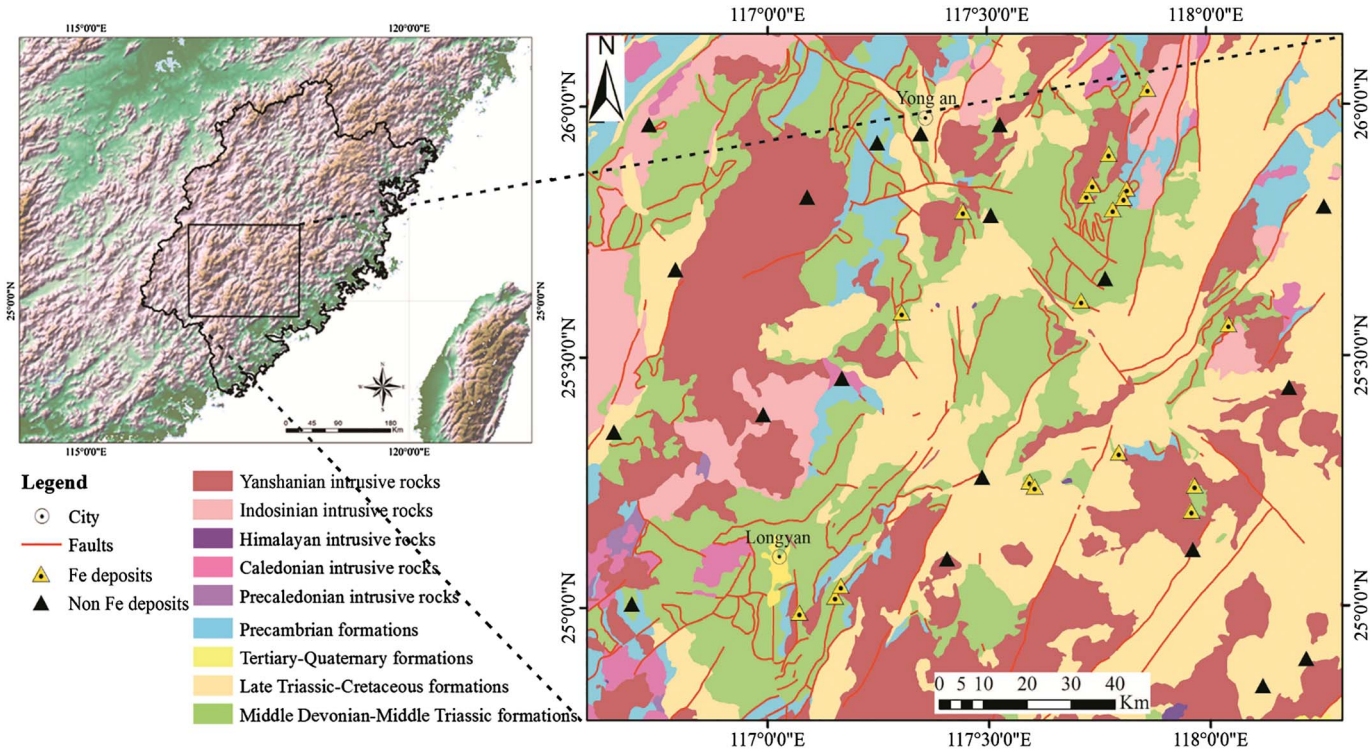

Fig. 1. Simplified geological map of southwestern Fujian Province, China. Compiled from China Geological Survey, 2011.

element associations and populations from multi-element geochemistry. The patterns associated with the third component were linked to Au related to the saprolitic soils potentially representing local epithermal processes associated with zones of dilation and the regional faulting. Zuo et al. (2013) unitized robust PCA to identify a meaningful elemental association. In the first principal component, positive loading may represent porphyry-type Cu–Mo mineralization associated with granites, and negative loadings may indicate hydrothermal-type Pb–Zn deposits. Yousefi (2017) applied the staged factor analysis to obtain two meaningful factors to reflect the presence of porphyry Cu deposits, Ag–Mo–Pb association and Cu–Zn association, respectively in the fourth and fifth stage factor analysis. The third approach involves application of spatial analysis for geochemical exploration based on geographic information system technology to extract useful elemental associations related to mineralization (Zuo and Wang, 2016; Zuo et al., 2016). Spatial analysis is widely applied in mapping mineral prospectivity. For example, Carranza (2009) and Parsa et al. (2017a) applied the distance distribution analysis (Berman, 1977, 1986) to measure the spatial association between a set of mineral deposit locations and a set of geological features; Yousefi and Carranza (2015a, 2015b) applied the prediction-area (P–A) plot to estimate the weights of each evidential map; Yousefi (2017) applied the P-A plot to evaluate the integrated geochemical signatures; Parsa et al. (2017b) applied the success rate curve (Agterberg and Bonham-Carter, 2005) to compare the two sets of multifractal and ordinary gridded geochemical data; Chen (2015) and Chen and Wu (2016) applied the Youden index to measure the spatial association between classified geochemical anomalies and discovered polymetallic deposits. Chen and Wu (2017) applied the receiver operating characteristic (ROC) technique to analyze the spatial relationships between geochemical patterns and locations of mineral deposits and then select the elemental association for mapping mineral prospectivity. Parsa et al. (2017d) applied the ROC to discriminate significant geochemical signatures. In the method reported in this study, an elemental association related to mineralization is identified by investigating geochemical patterns and measuring the spatial correlations between those patterns and known mineral deposits.

2. Methods

2.1. Multifractal spectra

Geochemical patterns can be modeled as fractals or multifractals. A multifractal model involves several concepts, including the partition function $\chi_q(\varepsilon)$, the mass exponent $\tau(q)$, the singularity exponent $a(q)$ and the multifractal spectrum $f(a)$. Let $\mu_i(\varepsilon)$ be the total concentration of an element μ in the ith cell of a linear scale ε. The partition function $\chi_q(\varepsilon)$ can be defined as (Evertsz and Mandelbrot, 1992)

$$\chi_q(\varepsilon) = \sum_{N(\varepsilon)} \mu_i{}^q(\varepsilon) \tag{1}$$

where $N(\varepsilon)$ is the total number of cells of size ε. If the distribution of $\mu_i(\varepsilon)$ is multifractal, the partition function of $\chi_q(\varepsilon)$ has a simple power-law relation with cell size ε for q with $-\infty \le q \le +\infty$, or

$$\chi_q(\varepsilon) \propto \varepsilon^{\tau(q)} \tag{2}$$

where $\propto$ represents proportionality, and $\tau(q)$ is the mass exponent of order q. The singularity exponent $a(q)$ and the multifractal spectrum can be obtained using the Legendre transformation (Evertsz and Mandelbrot, 1992),

$$a(q) = \frac{d\tau(q)}{q} \tag{3}$$

$$f[a(q)] = a(q)q - \tau(q) \tag{4}$$

The asymmetry index R has been defined as (Xie and Bao, 2004)

$$R = \frac{\alpha(0) - \alpha_{min}}{\alpha_{max} - \alpha(0)} \tag{5}$$

where $a(0)$ is the value of a when $q = 0$, and $a_{\min}$ and $a_{\max}$ represent the minimum and maximum values of the singularity index a, respectively. The asymmetry index can be used to quantify whether local

Table 1
Multifractal parameters of the studied elements.

Elements	$\alpha(0)$	α_{min}	α_{max}	$\alpha(0)-\alpha_{min}$	$\alpha_{max}-\alpha(0)$	$\alpha_{max}-\alpha_{min}$	R
Ag	2.05	0.65	2.40	1.40	0.35	1.75	3.98
Al_2O_3	2.01	1.92	2.79	0.09	0.79	0.87	0.11
As	2.08	0.82	3.03	1.26	0.95	2.21	1.32
Au	2.09	0.62	3.20	1.48	1.11	2.59	1.33
B	2.07	1.33	3.05	0.74	0.98	1.72	0.75
Ba	2.02	0.96	3.63	1.05	1.61	2.66	0.65
Be	2.02	0.88	2.40	1.15	0.37	1.52	3.08
Bi	2.10	0.69	3.30	1.41	1.20	2.60	1.17
CaO	2.04	1.01	2.18	1.03	0.14	1.17	7.15
Cd	2.08	1.40	2.67	0.68	0.59	1.26	1.15
Co	2.04	1.54	3.41	0.50	1.37	1.87	0.37
Cr	2.06	1.23	3.20	0.83	1.15	1.98	0.72
Cu	2.07	0.77	3.42	1.30	1.35	2.65	0.97
F	2.02	1.07	2.32	0.95	0.30	1.24	3.18
Fe_2O_3	2.01	0.93	2.30	1.08	0.28	1.36	3.84
Hg	2.04	0.38	3.52	1.65	1.48	3.13	1.12
K_2O	2.02	1.93	2.67	0.09	0.65	0.74	0.13
La	2.02	1.56	3.69	0.46	1.68	2.13	0.27
Li	2.02	1.37	2.37	0.65	0.35	1.00	1.85
MgO	2.02	0.21	2.74	1.81	0.72	2.53	2.51
Mn	2.03	1.58	3.65	0.45	1.62	2.07	0.28
Mo	2.06	1.04	2.60	1.02	0.54	1.56	1.87
Na_2O	2.09	0.45	2.70	1.64	0.62	2.25	2.66
Nb	2.02	1.79	3.37	0.23	1.36	1.58	0.17
Ni	2.06	1.15	3.39	0.91	1.33	2.24	0.69
P	2.03	1.27	2.82	0.76	0.79	1.55	0.96
Pb	2.05	1.14	2.76	0.91	0.71	1.62	1.29
Sb	2.05	0.72	2.91	1.33	0.86	2.19	1.55
SiO_2	2.00	1.99	2.01	0.01	0.01	0.02	0.69
Sn	2.06	1.30	2.48	0.76	0.42	1.18	1.79
Sr	2.02	1.77	2.25	0.26	0.23	0.48	1.12
Th	2.03	0.79	3.43	1.24	1.40	2.64	0.88
Ti	2.01	1.73	2.87	0.29	0.86	1.15	0.33
U	2.03	0.52	2.39	1.51	0.36	1.87	4.18
V	2.03	1.60	3.01	0.43	0.98	1.41	0.44
W	2.04	1.02	2.61	1.02	0.57	1.60	1.79
Y	2.01	1.76	2.14	0.26	0.13	0.38	1.99
Zn	2.03	0.64	2.41	1.39	0.38	1.77	3.65
Zr	2.02	1.81	2.72	0.20	0.71	0.91	0.29

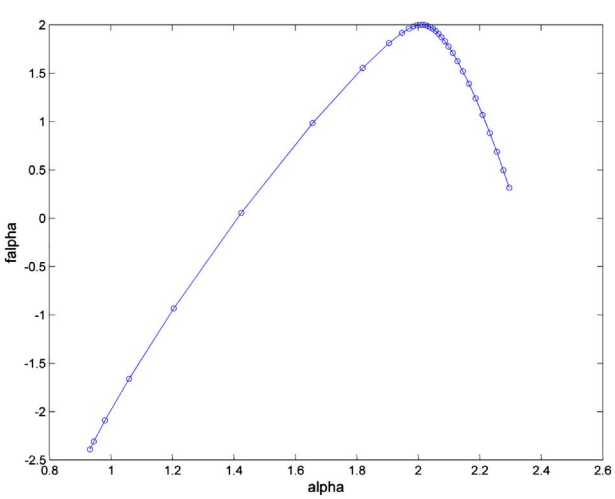

Fig. 2. A multifractal spectrum of Fe_2O_3.

enrichment or depletion pattern dominates in the study area. If $R > 1$, local enrichment plays a relatively more important role, whereas if $R < 1$, local depletion is predominant; if $R = 1$, these two locally variable patterns are of roughly equivalent importance. Further details about the multifractal model have been described by Evertsz and Mandelbrot (1992) and Cheng and Agterberg (1996).

2.2. Receiver operating characteristics (ROC)

The receiver operating characteristic (ROC) curve is a graph with the true positive rate on the *y*-axis and the false positive rate on the *x*-axis (Fawcett, 2006). This curve has been widely utilized in the machine learning community to evaluate the performance of predictive models. The area under the ROC curve (AUC), ranging from 0 to 1, was applied to evaluate the performance of mapping mineral prospectivity and geochemical anomalies (e.g., Nykänen et al., 2015, 2017; Chen and Wu, 2016, 2017; Parsa et al., 2017d). An AUC value of 0.5 suggests a random pattern; whereas an AUC value closer to 1 indicates better model performance.

Let x_i ($i = 1, 2, \ldots, p$) denote the predictive value of the ith true positive sample, and y_j ($j = 1,2, \ldots, n$) denote the predictive value of the jth true negative sample. The AUC can be calculated as (Bergmann et al., 2000):

$$AUC = \frac{1}{p \times n} \sum_{i=1}^{p} \sum_{j=1}^{n} \phi(x_i, y_j) \tag{6}$$

where

$$\phi(x_i, y_j) = \begin{cases} 1, x_i > y_j \\ 0.5, x_i = y_j \\ 0, x_i < y_j \end{cases} \tag{7}$$

The standard deviation of the AUC can be estimated as.

$$S_{AUC} = \sqrt{\frac{AUC(1 - AUC) + (p - 1)(Q_1 - AUC^2) + (n - 1)(Q_2 - AUC^2)}{p \times n}} \tag{8}$$

where

$$Q_1 = \frac{AUC}{2 - AUC} \text{ and } Q_2 = \frac{2AUC^2}{1 + AUC} \tag{9}$$

The value of Z_{AUC} can then be estimated as (Chen et al., 2014; Chen and Wu, 2016):

$$Z_{AUC} = \frac{AUC - 0.5}{S_{AUC}} \tag{11}$$

Here, Z_{AUC} is a random variable that satisfies standard normal distribution. Typically, if the value of Z_{AUC} is larger than 1.96, then the value of AUC is significantly different from AUC = 0.5.

3. Study area and data

The study area located in southwestern Fujian Province, China, in the southeastern interior of the Cathaysia Block, is well known for its extensive Mesozoic tectonic magmatism and accompanying Fe–Cu (Au)–Pb–Zn polymetallic mineralizations along the northeastern Yong'an–Meixian fold belt (Ge et al., 1981; Zhang et al., 2013). The geological evolution of this region involved clastic and carbonate sedimentation in the Hercynian epicontinental sea (D_3–P) over Caledonian and pre-Devonian basement, Indosinian W–E orogenic movement (T_1–T_2), early Yanshanian tectonic stress field transformation (T_3–J_2) and large-scale extension and magmatism (J_3–K_1) (Wu et al., 2000; Zhou and Li, 2000; Zhou et al., 2006; Sun et al., 2007; Shu et al., 2008; Li et al., 2012, 2013; Xu et al., 2013a, 2013b). Regionally, the dominant outcropping formations are late Paleozoic epicontinental sedimentary rocks: the Lower Carboniferous Lindi Formation (C_1l) and the Middle Carboniferous Jingshe Formation (C_2j). These typical marine interbedded clastic and carbonate sedimentary rocks, which are distributed discontinuously along the NE-trending Zhenghe–Dapu Fault, are closely associated with Fe polymetallic mineralization in the study area (Han and Ge, 1983; Zhang and Zuo, 2014; Zhang et al., 2015a, 2015b, 2015c; Wang Z. et al., 2015; Zuo et al., 2015; Zuo, 2016). The NE-trending

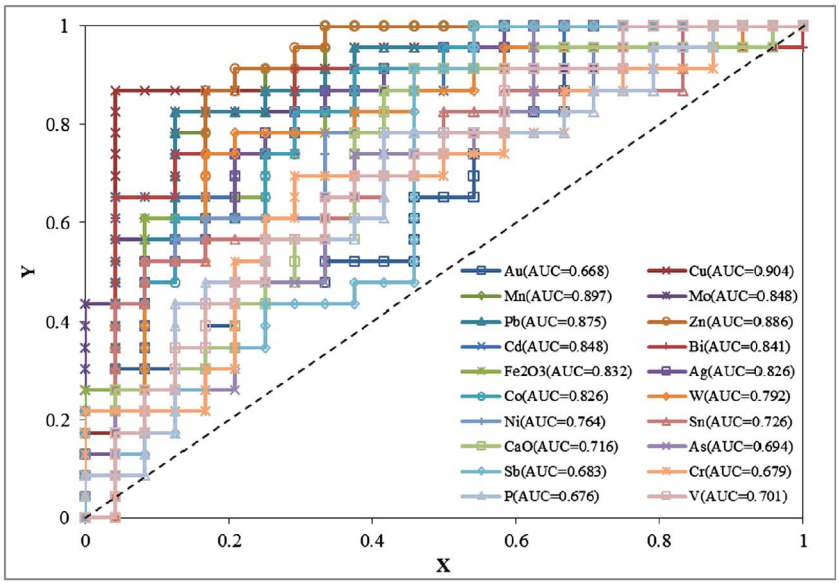

Fig. 3. ROC plots showing elements with strong spatial relationships with known Fe mineralization.

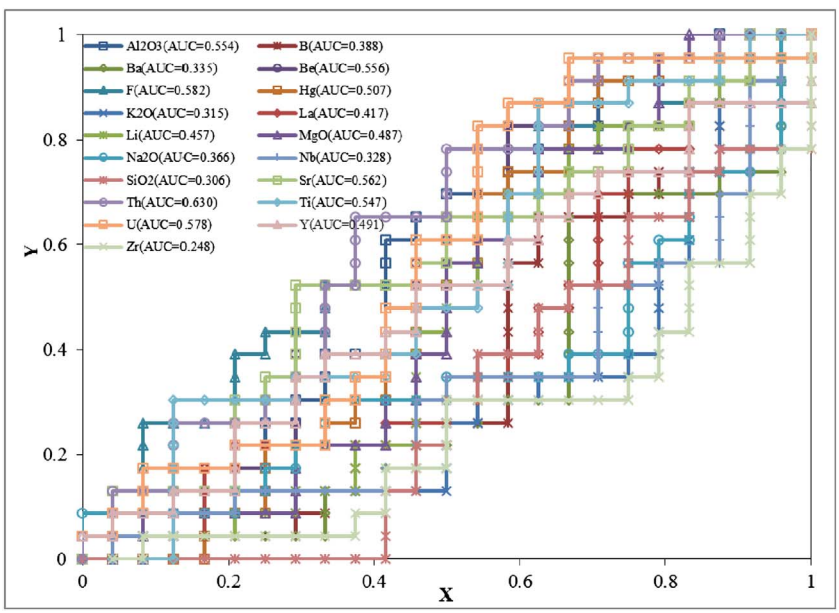

Fig. 4. ROC plots showing elements with negative spatial relationships with known Fe mineralization.

Zhenghe–Dafu Fault, the NW-trending Shanghang–Yunxiao Fault and the ENE-trending Nanping–Ninghua Fault, which form the boundaries of the study area, are the dominant fracture structures in this region. Based on correlative magmatic belt and geophysical seismic section data, the Zhenghe–Dapu Fault is a lithospheric fault. In addition, NE-trending Mesozoic nappe structures and fold belts that formed under compression during the early subduction of the paleo-Pacific plate are also primary regional structures (Kuo et al., 2016; Wang et al., 2017). Because of widespread tectono-magmatic activity, extensive plutonic rocks are widely distributed in this region; based on the timing of the associated tectonic movement, these rocks can be divided into Caledonian remelting granitoids, Hercynian–Indosinian remelting granitoids and Yanshanian granitoids. (Zhou and Li, 2000; Zhou et al., 2006; Mao, 2013). The ages obtained through zircon U–Pb dating of granitoids in Makeng (Dayang granites: 128–145 Ma, Zhang C. et al., 2012; 125–136 Ma, Wang S. et al., 2015; and Juzhou granite: 132 Ma, Wang S. et al., 2015), Luoyang (131–132 Ma, Zhang D. et al., 2012), Pantian (131 Ma, Lai et al., 2014), and Zhongjia (99 Ma, Yang et al., 2008) exhibit close temporal and spatial relationships with regional Fe polymetallic mineralization (Fig. 1).

The geochemical data used in this study were collected as part of the Chinese National Geochemical Mapping Project with a sampling density of one sample per 4 km^2 (Xie et al., 1997). The original geochemical data include 39 major and trace elements. The concentrations of these elements were mainly determined using inductively coupled plasma-mass spectrometry, X-ray fluorescence, and inductively coupled plasma-atomic emission spectrometry. The details of the detection limits and data quality have been discussed in Xie et al. (2008) and Wang et al. (2011). The dataset used in this study has been extensively explored in previous studies, and more information on this dataset can be found in the corresponding publications (Wang H. and Zuo, 2015; Wang H. et al., 2015a, 2015b; Xiong and Zuo, 2016, 2017).

4. Results and discussion

A MATLAB-based program for processing geochemical data using fractal/multifractal modeling software developed by Wang J. and Zuo (2015) was applied to preprocess the original geochemical data and to

Table 2
Values of AUC and Z_{AUC} of the studied elements.

Elements	AUC	Z_{AUC}
Ag	0.83	5.28
Al_2O_3	0.55	0.64
As	0.69	2.50
Au	0.67	2.12
B	0.39	− 1.36
Ba	0.34	− 2.08
Be	0.56	0.66
Bi	0.84	5.73
CaO	0.72	2.85
Cd	0.85	5.98
Co	0.83	5.28
Cr	0.68	2.28
Cu	0.90	8.66
F	0.58	0.97
Fe_2O_3	0.83	5.44
Hg	0.51	0.09
K_2O	0.32	− 2.38
La	0.42	− 1.00
Li	0.46	− 0.51
MgO	0.49	− 0.15
Mn	0.90	8.21
Mo	0.85	5.98
Na_2O	0.37	− 1.65
Nb	0.33	− 2.19
Ni	0.76	3.76
P	0.68	2.23
Pb	0.88	7.08
Sb	0.68	2.34
SiO_2	0.31	− 2.52
Sn	0.73	3.04
Sr	0.56	0.73
Th	0.63	1.60
Ti	0.55	0.56
U	0.58	0.93
V	0.70	2.62
W	0.79	4.36
Y	0.49	− 0.11
Zn	0.89	7.60
Zr	0.25	− 3.53

calculate the multifractal parameters listed in Table 1. Taking Fe_2O_3 as an example, a_{min}, $a(0)$, and a_{max} are 0.93, 2.01, and 2.30, respectively, calculated based on the multifractal spectrum (Fig. 2). The range of a_{max} and a_{min}, denoted Δa, is 1.36. This variable indicates the complexity of the geochemical pattern; larger values of $\Delta\alpha$ represent greater geochemical pattern complexity. The R value of Fe_2O_3 calculated based on Eq. (5) is 3.84. Because this value is larger than 1, it suggests a left deviation for the multifractal spectrum curve of Fe_2O_3, which indicates that local enrichment in the spatial distribution of Fe_2O_3 is dominant in the study area.

Multifractal spectrum parameters for all of the studied elements are listed in Table 1. The elements Ag, As, Au, Be, Bi, CaO, Cd, F, Fe_2O_3, Hg, Li, MgO, Mo, Na_2O, Pb, Sb, Sn, Sr, U, W, Y, and Zn have R values > 1, suggesting that these elements are enriched in the study area from a multifractal viewpoint. The R values of the other elements are below 1, suggesting that they are depleted. Among the 39 elements, Hg and SiO_2 yield the maximum (3.13) and minimum (0.02) values of Δa. Hg is therefore associated with greater complexity in spatial distribution, which is attributed to its geochemical behavior and the structure of the widely distributed fault system, whereas SiO_2 is associated with a more regular geochemical pattern because intrusions with consistent SiO_2 content are widely developed in the study area.

To draw a ROC curve, true positive and negative samples are required. The known mineral deposits can be regarded as the true positive samples. Typically, randomly simulated points are selected as true negative samples. However, other types of known mineral deposits or barren drill holes can also be employed as true negative samples (Nykänen et al., 2015). In this study, 19 known skarn Fe deposits and 19 random points are assigned as true positive and negative samples, respectively (see Fig.1). The resulting ROC curve (Figs. 3 and 4; Table 2) shows that the AUC values of Hg, MgO, and Y approach 0.5, which indicate that these three elements do not correlate spatially with Fe mineralization. The elements Cu, Mn, Pb, and Zn have high AUC values, close to 0.9, which demonstrate strong spatial correlations with skarn Fe mineralization. The elements Ba, K_2O, Nb, SiO_2 and Zr have low AUC values near 0.3, which suggest that these five elements have negative spatial correlation with skarn Fe mineralization. These

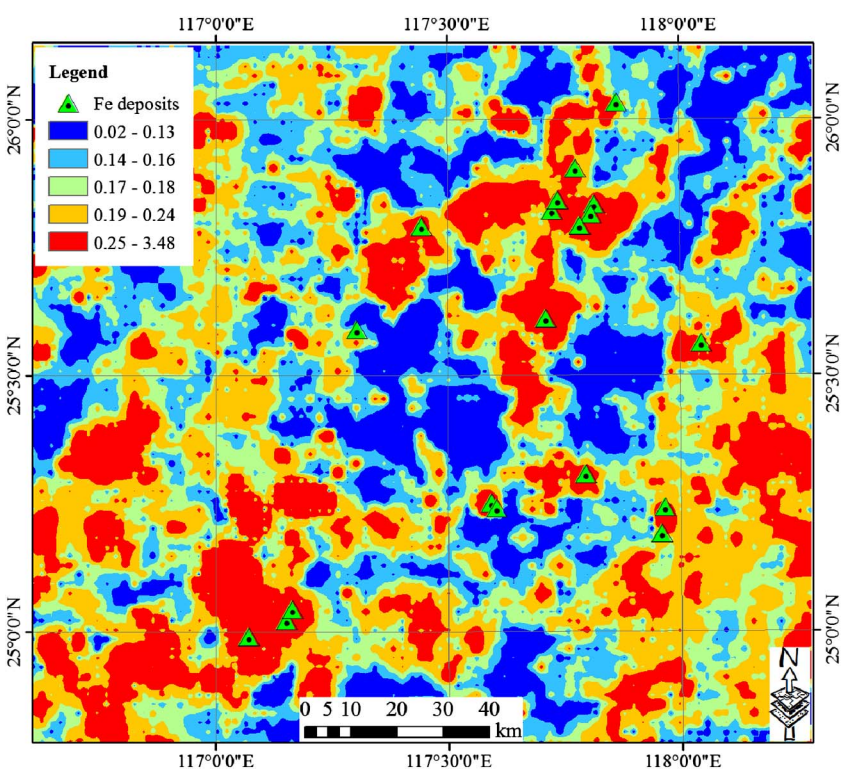

Fig. 5. Integrated geochemical map based on the identified elemental association related to skarn Fe mineralization.

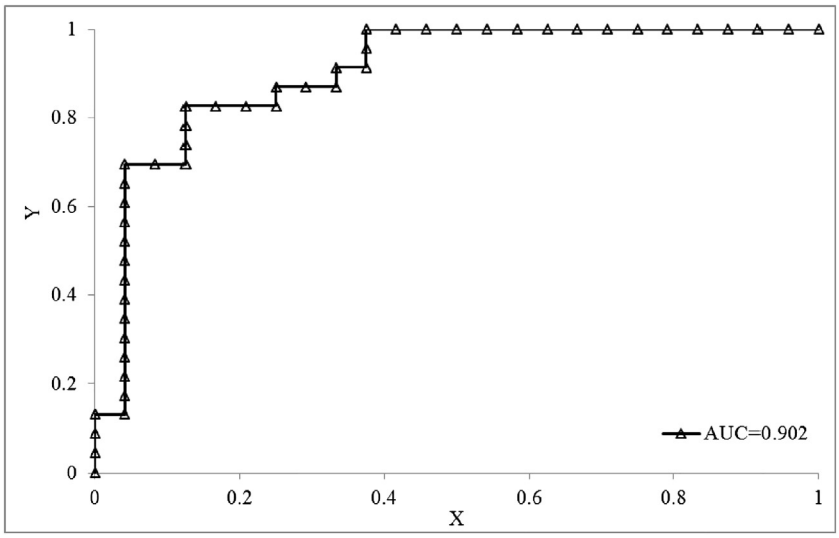

Fig. 6. A ROC plot showing the spatial relationship between the integrated geochemical map and known mineralization.

patterns are also important for the formation of mineralization as Liu et al. (2016) reported that the extent of the negative Na_2O anomaly represented the fluid-rock interaction zones.

The AUC values of 28 elements, Ag, Al_2O_3, As, Au, Be, Bi, CaO, Cd, Co, Cr, Cu, F, Fe_2O_3, Hg, Mn, Mo, Ni, P, Pb, Sb, Sn, Sr, Th, Ti, U, V, Zn, and W, are larger than 0.5, whereas the AUC values of the other elements are lower than 0.5. The Z_{AUC} values of 20 elements, Ag, As, Au, Bi, CaO, Cd, Co, Cr, Cu, Fe_2O_3, Mn, Mo, Ni, P, Pb, Sb, Sn, V, W, and Zn, are larger than 1.96, which indicates that these elements are spatially correlated with known Fe mineral deposits at the 95% confidence level.

In terms of values of R, AUC and Z_{AUC}, the elemental association of Ag, As, Au, Bi, CaO, Cd, Fe_2O_3, Mo, Pb, Sb, Sn, W, and Zn is favorable for indicating skarn Fe-related mineralization. The ranking order of these elements from largest to smallest AUC value is Zn (0.89) > Pb (0.88) > Mo (0.85) = Cd (0.85) > Bi (0.84) > Fe_2O_3 (0.83) = Ag (0.83) > W (0.79) > Sn (0.73) > CaO (0.72) > As (0.69) > Sb (0.68) > Au (0.67), which represents a spatial correlation sequence between geochemical patterns and known skarn Fe mineralization. Of these selected elements, Zn, Pb and Fe_2O_3 were selected based on experience and field observations for geochemical prospecting (Wang H. and Zuo, 2015, Wang J. and Zuo, 2015; Zuo et al., 2015; Xiong and Zuo, 2016, 2017). These results can guide geochemists to select pathfinder elements for further geochemical exploration in the study area.

A simple method was used to produce an integrated geochemical map based on the identified elemental association related to skarn Fe mineralization. The concentrations of elements of this elemental association were first normalized into the range [0, 1] to eliminate influence of dimension. The normalized values for each element map were then added together to create an integrated geochemical map (union score map) (Fig. 5). This map is a mixed pattern and should be further decomposed for delineating geochemical targets in future. A ROC curve was produced based on the integrated geochemical map and known skarn mineral deposits. The AUC value for the resulting map reaches 0.902 with a Z_{AUC} value of 8.53 (Fig. 6), which indicates that this integrated geochemical map can be employed as a reference for discovering skarn Fe-related mineralization in the study area. The AUC value of the integrated geochemical map is larger than the AUC value for any individual element in the elemental association, which implies that the integrated map can improve the ability of this method for indicating mineralization. This finding suggests that the identified elemental association related to skarn Fe mineralization is meaningful for geochemical prospecting.

5. Conclusions

In this study, a hybrid method based on integrating the multifractal spectrum and ROC curve was applied to identify an elemental association related to mineralization for geochemical prospecting via spatial analysis using a case study from southwestern Fujian Province, China. The following conclusion were obtained:

(1) The elemental association of Ag, As, Au, Bi, CaO, Cd, Fe_2O_3, Mo, Pb, Sb, Sn, W, and Zn can indicate occurrences of skarn Fe mineralization. The ranking order of the spatial correlations with known Fe deposits, from strongest to weakest correlation, is Zn (0.89) > Pb (0.88) > Mo (0.85) = Cd (0.85) > Bi (0.84) > Fe_2O_3 (0.83) = Ag (0.83) > W (0.79) > Sn (0.73) > CaO (0.72) > As (0.69) > Sb (0.68) > Au (0.67). This elemental association and ranking sequence can guide selection of elements for new discovery of skarn Fe mineralization in the study area; and.

(2) The proposed hybrid method based on spatial analysis provides objective selection criteria for elemental associations related to mineralization for geochemical prospecting.

It should be noted that the proposed apporach should be in conjunction with the geological environment for the formation of mineralization. In addition, further studies of typical mineral deposits can help in selecting elemental associations. Besides, the proposed method is only suitable in the well-explored area in which a few mineral deposits are discovered.

Acknowledgements

A part of this study was presented at 2017 Goldschmidt Conference in Paris. The author thanks John Carranza for his edits, and two reviewers' comments and suggestions, which improved this study. Thanks are due to Jian Wang and Yihui Xiong from the China University of Geosciences for processing part of data. This research was supported in part by the National Natural Science Foundation of China under Grants 41772344 and 41522206, the Natural Science Foundation of Hubei Province (China) under Grant 2017CFA053, and the MOST Special Fund from the State Key Laboratory of Geological Processes and Mineral Resources, China University of Geosciences under Grant MSFGPMR03-3.

References

Agterberg, F.P., Bonham-Carter, G.F., 2005. Measuring the performance of mineral-potential maps. Nat. Resour. Res. 14, 1–17.
Bergmann, R., Ludbrook, J., Spooren, W.P.J.M., 2000. Different outcomes of the

Wilcoxon–Mann–Whitney test from different statistics packages. Am. Stat. 54, 72–77.
Berman, M., 1977. Distance distributions associated with Poisson processes of geometric figures. J. Appl. Probab. 14, 195–199.
Berman, M., 1986. Testing for spatial association between a point processes and another stochastic process. Appl. Stat. 35, 54–62.
de Caritat, P., Cooper, M., Pappas, W., Thun, C., Webber, E., 2010. National Geochemical Survey of Australia: Analytical Methods Manual Geoscience Australia Record. (2010/15 (22 pp.)).
Carranza, E.J.M., 2009. Controls on mineral deposit occurrence inferred from analysis of their spatial pattern and spatial association with geological features. Ore Geol. Rev. 35, 383–400.
Chen, Y., 2015. Mineral potential mapping with a restricted Boltzmann machine. Ore Geol. Rev. 71, 749–760.
Chen, Y., Wu, W., 2016. A prospecting cost-benefit strategy for mineral potential mapping based on ROC curve analysis. Ore Geol. Rev. 74, 26–38.
Chen, Y., Wu, W., 2017. Mapping mineral prospectivity using an extreme learning machine regression. Ore Geol. Rev. 80, 200–213.
Chen, Y., Lu, L., Li, X., 2014. Application of continuous restricted Boltzmann machine to identify multivariate geochemical anomaly. J. Geochem. Explor. 140, 56–63.
Chen, S., Hattori, K., Grunsky, E.C., 2016. Multivariate statistical analysis of the REE-mineralization of the maw zone, Athabasca Basin, Canada. J. Geochem. Explor. 161, 98–111.
Cheng, Q., 2007. Mapping singularities with stream sediment geochemical data for prediction of undiscovered mineral deposits in Gejiu, Yunnan Province, China. Ore Geol. Rev. 32, 314–324.
Cheng, Q., Agterberg, F.P., 1996. Multifractal modeling and spatial statistics. Math. Geol. 28, 1–16.
Darnley, A.G., Björklund, A., Bölviken, B., Gustavsson, N., Koval, P.V., Plant, J.A., Steenfelt, A., Tauchid, M., Xie, X., Garrett, R.G., Hall, G.E.M., 1995. A Global Geochemical Database for Environmental and Resource Management Final Report of IGCP Project 259, Earth Sciences, 19. UNESCO Publishing, Paris.
Evertsz, C.J.G., Mandelbrot, B.B., 1992. Multifractal Measures (Appendix B). In: Peitgen, H.O., Jurgens, H., Saupe, D. (Eds.), Chaos and Fractals. Springer Verlag, New York, pp. 922–953.
Fawcett, T., 2006. An introduction to ROC analysis. Pattern Recogn. Lett. 27, 861–874.
Ge, C., Han, F., Zhou, T., Chen, D., 1981. Geological characteristics of the Makeng iron deposit of marine volcano-sedimentary origin. Acta Geosci. Sin. 3, 47–69 (in Chinese with English Abstract).
Grunsky, E.C., 1986. Recognition of alteration in volcanic rocks using statistical analysis of lithogeochemical data. J. Geochem. Explor. 25, 157–183.
Grunsky, E.C., Smee, B.W., 1999. The differentiation of soil types and mineralization from multi-element geochemistry using multivariate methods and digital topography. J. Geochem. Explor. 67, 287–299.
Grunsky, E.C., Drew, L.J., Woodruff, L.G., Friske, P.W.B., Sutphin, D.M., 2013. Statistical variability of the geochemistry and mineralogy of soils in the maritime provinces of Canada and part of the northeast United States. Geochem. Explor. Environ. Anal. 13, 249–266.
Grunsky, E.C., Mueller, U.A., Corrigan, D., 2014. A study of the lake sediment geochemistry of the Melville peninsula using multivariate methods: applications for predictive geological mapping. J. Geochem. Explor. 141, 15–41.
Grunsky, E.C., De Caritat, P., Mueller, U.A., 2017. Using surface regolith geochemistry to map the major crustal blocks of the Australian continent. Gondwana Res. 46, 227–239.
Han, F., Ge, C., 1983. Geological and geochemical features of submarine volcanic hydrothermal-sedimentary mineralization of Makeng iron deposit, Fujian Province. Bull. Inst. Mineral Deposits Chin. Acad. Geol. Sci. 7, 1–118 (in Chinese with English abstract).
Harris, J.R., Wilkinson, L., Grunsky, E., Heather, K., Ayer, J., 1999. Techniques for analysis and visualization of lithogeochemical data with applications to the Swayze greenstone belt, Ontario. J. Geochem. Explor. 67, 301–334.
Harris, J.R., Wilkinson, L., Grunsky, E.C., 2000. Effective use and interpretation of lithogeochemical data in regional mineral exploration programs: application of geographic information systems (GIS) technology. Ore Geol. Rev. 16, 107–143.
Kuo, Y., Wang, C., Kuo-Chen, H., Jin, X., Cai, H., Lin, J., Wu, F.T., Yen, H., Huang, B., Liang, W., Okaya, D., Brown, L., 2016. Crustal structures from the Wuyi-Yunkai orogen to the Taiwan orogen: the onshore-offshore wide-angle seismic experiments of the TAIGER and ATSEE projects. Tectonophysics 692, 164–180.
Lai, S., Chen, R., Zhang, D., Di, Y., Gong, Y., Yuan, Y., Chen, L., 2014. Petrogeochemical features and zircon LA-ICP-MS U–Pb ages of granite in the Pantian iron ore deposit, Fujian province and their relationship with mineralization. Acta Petrol. Sin. 30, 1780–1792 (in Chinese with English abstract).
Li, Z., Li, X., Chung, S., Lo, C., Xu, X., Li, W., 2012. Magmatic switch-on and switch-off along the South China continental margin since the Permian: transition from an Andean-type to a western Pacific-type plate boundary. Tectonophysics 532, 271–290.
Li, P., Yu, X., Li, H., Qiu, J., Zhou, X., 2013. Jurassic–cretaceous tectonic evolution of Southeast China: geochronological and geochemical constraints of Yanshanian granitoids. Int. Geol. Rev. 55, 1202–1219.
Liu, Y., Ma, S., Zhu, L., Sadeghi, M., Doherty, A.L., Cao, D., Le, C., 2016. The multi-attribute anomaly structure model: an exploration tool for the Zhaojikou epithermal Pb-Zn deposit, China. J. Geochem. Explor. 169, 50–59.
Mao, J., 2013. Mesozoic-Cenozoic Magmatism and Mineralization in South China Block (SCB) and Adjacent Region. China Science Press (CSPM) (In Chinese with English abstract).
Mueller, U.A., Grunsky, E.C., 2016. Multivariate spatial analysis of lake sediment geochemical data; Melville peninsula, Nunavut, Canada. Appl. Geochem. 75, 247–262.
Nykänen, V., Lahti, I., Niiranen, T., Korhonen, K., 2015. Receiver operating characteristics (ROC) as validation tool for prospectivity models—a magmatic Ni–Cu case study from the Central Lapland Greenstone Belt, northern Finland. Ore Geol. Rev. 71, 853–860.
Nykänen, V., Niiranen, T., Molnár, F., Lahti, I., Korhonen, K., Cook, N., Skyttä, P., 2017. Optimizing a knowledge-driven Prospectivity model for gold deposits within Peräpohja Belt, northern Finland. Nat. Resour. Res. 26, 571–584.
Parsa, M., Maghsoudi, A., Yousefi, M., 2017a. An improved data-driven fuzzy mineral prospectivity mapping procedure; cosine amplitude-based similarity approach to delineate exploration targets. Int. J. Appl. Earth Obs. Geoinf. 58, 157–167.
Parsa, M., Maghsoudi, A., Yousefi, M., Carranza, E.J.M., 2017b. Multifractal interpolation and spectrum–area fractal modeling of stream sediment geochemical data: implications for mapping exploration targets. J. Afr. Earth Sci. 128, 5–15.
Parsa, M., Maghsoudi, A., Carranza, E.J.M., Yousefi, M., 2017c. Enhancement and mapping of weak multivariate stream sediment geochemical anomalies in Ahar area, NW Iran. Nat. Resour. Res. 26, 443–455.
Parsa, M., Maghsoudi, A., Yousefi, M., 2017d. A receiver operating characteristics-based geochemical data fusion technique for targeting undiscovered mineral deposits. Nat. Resour. Res. http://dx.doi.org/10.1007/s11053-017-9351-6.
Shu, L., Faure, M., Wang, B., Zhou, X., Song, B., 2008. Late Palaeozoic-Early Mesozoic geological features of South China: response to the Indosinian collision events in Southeast Asia. Compt. Rendus Geosci. 340, 151–165.
Sun, W., Ding, X., Hu, Y., Li, X., 2007. The golden transformation of the cretaceous plate subduction in the west Pacific. Earth Planet. Sci. Lett. 262, 533–542.
Wang, H., Zuo, R., 2015. A comparative study of trend surface analysis and spectrum-area multifractal model to identify geochemical anomalies. J. Geochem. Explor. 155, 84–90.
Wang, J., Zuo, R., 2015. A MATLAB-based program for processing geochemical data using fractal/multifractal modeling. Earth Sci. Inf. 8, 937–947.
Wang, X., Xie, X., Zhang, B., Hou, Q., 2011. Geochemical probe into China's continental crust. Acta Geosci. Sin. 32, 65–83 (In Chinese with English abstract).
Wang, S., Zhang, D., Vatuva, A., Yan, P., Ma, S., Feng, H., Yu, T., Bai, Y., Di, Y., 2015. Zircon U-Pb Geochronology, Geochemistry and Hf Isotope Compositions of the Dayang and Juzhou Granites in Longyan, Fujian and Their Geological Implications. 44. pp. 450–468 (In Chinese with English abstract).
Wang, Z., Zuo, R., Zhang, Z., 2015. Spatial analysis of Fe deposits in Fujian Province, China: implications for mineral exploration. J. Earth Sci. 26, 813–820.
Wang, H., Cheng, Q., Zuo, R., 2015a. Quantifying the spatial characteristics of geochemical patterns via GIS-based geographically weighted statistics. J. Geochem. Explor. 157, 110–119.
Wang, H., Cheng, Q., Zuo, R., 2015b. Spatial characteristics of geochemical patterns related to Fe mineralization in the southwestern Fujian province (China). J. Geochem. Explor. 148, 259–269.
Wang, S., Zhang, D., Wu, G., Vatuva, A., Di, Y., Yan, P., Feng, H., Ma, S., 2017. Late Paleozoic to Mesozoic extension in southwestern Fujian Province, South China: geochemical, geochronological and Hf isotopic constraints from basic-intermediate dykes. Geosci. Front. 8, 529–540.
Wu, G., Zhang, D., Chen, B., Wu, J., 2000. Transformation of Mesozoic tectonic domain and its relation to mineralization in southeastern China: an evidence of southwestern Fujian Province. Earth Sci. J. China Univ. Geosci. 25, 390–396 (In Chinese with English abstract).
Xie, S., Bao, Z., 2004. Fractal and multifractal properties of geochemical fields. Math. Geol. 36, 847–864.
Xie, X., Mu, X., Ren, T., 1997. Geochemical mapping in China. J. Geochem. Explor. 60, 99–113.
Xie, X., Wang, X., Zhang, Q., Xu, S., 2008. Multi-scale geochemical mapping in China. Geochem. Explo. Environ. Anal. 8, 333–341.
Xiong, Y., Zuo, R., 2016. Recognition of geochemical anomalies using a deep autoencoder network. Comput. Geosci. 86, 75–82.
Xiong, Y., Zuo, R., 2017. Effects of misclassification costs on mapping mineral prospectivity. Ore Geol. Rev. 82, 1–9.
Xu, Z., Cheng, R., Wang, L., Zhang, L., Shen, Y., Yu, Z., 2013a. Mineralogical and element geochemical characteristics of the Late Triassic-Middle Jurassic sedimentary rocks in southwestern Fujian Province: constraints on changes of basin tectonic settings. Acta Petrol. Sin. 29, 2913–2924.
Xu, Z., Cheng, R., Zhang, L., Wang, L., 2013b. Transgression-regression event element geochemistry records of southwestern Fujian in Late Triassic-Middle Jurassic. J. Cent. South Univ. 20, 2819–2829.
Yang, Z., Zhang, D., Feng, C., She, H., Li, J., 2008. SHRIMP zircon U–Pb dating of quartz porphyry from Zhongjia tin–polymetallic deposit in Longyan area, Fujian Province, and its geological significance. Mineral Deposits 27, 329–335 (in Chinese with English Abstract).
Yousefi, M., 2017. Recognition of an enhanced multi-element geochemical signature of porphyry copper deposits for vectoring into mineralized zones and delimiting exploration targets in Jiroft area, SE Iran. Ore Geol. Rev. 83, 200–214.
Yousefi, M., Carranza, E.J.M., 2015a. Fuzzification of continuous-value spatial evidence for mineral prospectivity mapping. Comput. Geosci. 74, 97–109.
Yousefi, M., Carranza, E.J.M., 2015b. Prediction-area (P-A) plot and C-A fractal analysis to classify and evaluate evidential maps for mineral prospectivity modelling. Comput. Geosci. 79, 69–81.
Zhang, Z., Zuo, R., 2014. Sr–Nd–Pb isotope systematics of magnetite: implications for the genesis of Makeng Fe deposit, southern China. Ore Geol. Rev. 57, 53–60.
Zhang, C., Li, L., Zhang, C., Wang, J., 2012. LA-ICP-MS zircon U-Pb ages and Hf isotopic compositions of Dayang granite from Longyan, Fujian Province. Geoscience 434–444 (in Chinese with English abstract), 26.
Zhang, D., Wu, G., Di, Y., Wang, C., Yao, J., Zhang, Y., Lv, L., Yuan, Y., Shi, J., 2012. Geochronology of diagenesis and mineralization of the Luoyang iron deposit in

Zhangping city, Fujian province and its geological significance. Earth Sci. J. China Univ. Geosci. 37, 1217–1231.
Zhang, D., Wu, G., Di, Y., Yu, X., Shi, Y., Zhang, X., Wang, Q., Huang, H., 2013. SHRIMP U-Pb zircon geochronology and Nd-Sr isotopic study of the Mamianshan group: implications for the Neoproterozoic tectonic development of southeast China. Int. Geol. Rev. 55, 730–748.
Zhang, Z., Zuo, R., Cheng, Q., 2015a. The mineralization age of the Makeng Fe deposit, South China: implications from U-Pb and Sm-Nd geochronology. Int. J. Earth Sci. 104, 663–682.
Zhang, Z., Zuo, R., Cheng, Q., 2015b. Geological features and formation processes of the Makeng Fe deposit, China. Resour. Geol. 65, 266–284.
Zhang, Z., Zuo, R., Xiong, Y., 2015c. A comparative study of fuzzy weights of evidence and random forests for mapping mineral prospectivity for skarn-type Fe deposits in the southwestern Fujian metallogenic belt, China. Sci. China Earth Sci. 59, 556–572.
Zhou, X., Li, W., 2000. Origin of Late Mesozoic igneous rocks in southeastern China: implications for lithosphere subduction and underplating of mafic magmas. Tectonophysics 326, 269–287.
Zhou, X., Sun, T., Shen, W., Shu, L., Niu, Y., 2006. Petrogenesis of Mesozoic granitoids and volcanic rocks in South China: a response to tectonic evolution. Episodes 29, 26–33.
Zuo, R., 2016. A nonlinear controlling function of geological features on magmatic–hydrothermal mineralization. Sci Rep 6, 27127.
Zuo, R., 2017. Machine learning of mineralization-related geochemical anomalies: a review of potential methods. Nat. Resour. Res. 26, 457–464.
Zuo, R., Wang, J., 2016. Fractal/multifractal modeling of geochemical data: a review. J. Geochem. Explor. 164, 33–41.
Zuo, R., Cheng, Q., Agterberg, F.P., Xia, Q., 2009. Application of singularity mapping technique to identification local anomalies using stream sediment geochemical data, a case study from Gangdese, Tibet, western China. J. Geochem. Explor. 101, 225–235.
Zuo, R., Xia, Q., Wang, H., 2013. Compositional data analysis in the study of integrated geochemical anomalies associated with mineralization. Appl. Geochem. 28, 202–211.
Zuo, R., Zhang, Z., Zhang, D., Carranza, E.J.M., Wang, H., 2015. Evaluation of uncertainty in mineral prospectivity mapping due to missing evidence: a case study with skarn-type Fe deposits in southwestern Fujian Province, China. Ore Geol. Rev. 71, 502–515.
Zuo, R., Carranza, E.J.M., Wang, J., 2016. Spatial analysis and visualization of exploration geochemical data. Earth Sci. Rev. 158, 9–18.